J. Fluid Mech. (2011), *vol.* 673, *pp.* 406–431. © Cambridge University Press 2011
doi:10.1017/S002211201000635X

Interaction between two spherical bubbles rising in a viscous liquid

YANNICK HALLEZ[1] AND DOMINIQUE LEGENDRE[2,3]†

[1]Université de Toulouse, INPT, UPS, LGC (Laboratoire de Génie Chimique), 118 route de Narbonne, F-31062 Toulouse CEDEX 9, France

[2]Université de Toulouse, INPT, UPS, IMFT (Institut de Mécanique des Fluides de Toulouse), Allée Camille Soula, F-31400 Toulouse, France

[3]CNRS, IMFT, F-31400 Toulouse, France

(Received 14 June 2010; revised 30 October 2010; accepted 4 December 2010; first published online 2 March 2011)

The three-dimensional flow around two spherical bubbles moving in a viscous fluid is studied numerically by solving the full Navier–Stokes equations. The study considers the interaction between two bubbles for moderate Reynolds numbers ($50 \leqslant Re \leqslant 500$, Re being based on the bubble diameter) and for positions described by the separation S ($2.5 \leqslant S \leqslant 10$, S being the distance between the bubble centres normalised by the bubble radius) and the angle θ ($0^\circ \leqslant \theta \leqslant 90^\circ$) formed between the centreline and the direction perpendicular to the direction of the motion. We provide a general description of the interaction extending the results obtained for two bubbles moving side by side ($\theta = 0^\circ$) by Legendre, Magnaudet & Mougin (*J. Fluid Mech.*, vol. 497, 2003, p. 133) and for two bubbles moving in line ($\theta = 90^\circ$) by Yuan & Prosperetti (*J. Fluid Mech.*, vol. 278, 1994, p. 325). Simple models based on physical arguments are given for the drag and lift forces experienced by each bubble. The interaction is the combination of three effects: a potential effect, a viscous correction (Moore's correction) and a significant wake effect observed on both the drag and the transverse forces of the second bubble when located in the wake of the first one.

Key words: bubble dynamics

1. Introduction

Most of the bubbly flows observed in industrial processes as well as in natural events can involve locally large concentrations of bubbles. The use of models developed for a single bubble is not satisfactory since interactions between bubbles are not considered. The first step in considering hydrodynamic bubble interactions is to understand and develop models for pair interaction. The objective of this work is to consider bubble pair interactions for intermediate to large rising bubble Reynolds numbers, typically $Re \geqslant O(10)$.

For this range of Reynolds numbers, the motion of a single bubble has been extensively studied (see Clift, Grace & Weber 1978; Magnaudet & Eames 2000). The first significant understanding of the correct derivation of the terminal velocity was addressed by Levich (1962). Using a global energy balance, Levich (1962) deduced the drag force $\boldsymbol{F_D} = -12\pi\mu R\boldsymbol{U_b}$ from the dissipation induced by the

† Email address for correspondence: legendre@imft.fr

https://doi.org/10.1017/S002211201000635X Published online by Cambridge University Press

potential flow generated by a rising bubble, the corresponding drag coefficient being $C_D = F_D/\frac{1}{2}\pi R^2 \rho U_b^2 = 48/Re$, where μ is the fluid viscosity, R is the bubble radius, U_b is its terminal rising velocity and $Re = 2R\rho U_b/\mu$ is the rising bubble Reynolds number. This is called viscous potential flow approximation (Joseph & Wang 2004; Joseph 2006*a*,*b*). The potential flow assumption is valid everywhere except at the bubble surface where the zero-shear stress condition generates an interfacial distribution of vorticity $\Omega = O(3U_b/R)$. The Levich drag force is thus valid in the limit $Re \to \infty$. Moore (1963) considered the diffusion and transport in the wake of the vorticity produced at the bubble surface. Considering a weak viscous boundary layer and a thin wake, he obtained $C_{D\infty} = 48/Re[1 - M_\infty/Re^{1/2}]$, showing that the induced effect of vorticity is a drag reduction. The term containing $M_\infty = 2.211$ is the so-called Moore correction for a single bubble. This expression has been clearly confirmed by the use of direct numerical simulations, which also indicate that it can be considered valid for $Re > 50$ (see Magnaudet & Eames 2000).

In the limit of irrotational flow ($Re = \infty$), several investigations based on the pioneering works of Jeffrey (1973) and van Wijngaarden (1976) have considered the interaction between two spheres (see for example Kok 1993 and references therein). Following the global kinetic energy balance proposed by Levich (1962), Kok (1993) used the potential flow solution to derive the viscous drag force for two spherical bubbles in interaction. The total force acting on the bubble (potential interaction and viscous drag) is valid in the limit $Re = \infty$, and was used to show that when a pair of bubbles rise in a quiescent liquid due to buoyancy, the bubbles are attracted towards (resp. repelled from) each other when the angle between their centrelines and the direction of motion is in (resp. out of) the range $[\theta_a, 180^\circ - \theta_a]$, θ_a being a critical angle ranging from 35.0°, when the two bubbles are in contact, to 54.7°, when they are widely separated. It was also established that only two steady situations can be observed: the first one is two bubbles rising side by side in contact, their centrelines being perpendicular to the rise velocity, and the second one is an infinite separating distance. Note that using the same approach, the case of growing bubbles rising in line was considered by Harper (2001).

The non-irrotational situation was considered analytically by Harper (1970, 1997) for two bubbles moving in line. Harper (1997) revisited his first work after the direct numerical simulations (DNS) of Yuan & Prosperetti (1994) for $Re = 20$, 50, 100 and 200. In this particular axisymmetric configuration, the potential solution (Kok 1993) predicts a drag increase of the trailing bubble (or second bubble noted using subscript 2) relative to the drag of the leading bubble (or first bubble noted using subscript 1):

$$C_{D1} = \frac{48}{Re}[1 - 2S^{-3} + 3S^{-6} + \cdots] - 12S^{-4} + 24S^{-7} + \cdots, \tag{1.1}$$

$$C_{D2} = \frac{48}{Re}[1 - 2S^{-3} + 3S^{-6} + \cdots] + 12S^{-4} - 24S^{-7} + \cdots, \tag{1.2}$$

where $S = d/R$ is the normalised separating distance. Note that in the present work the terms 'drag' and 'lift' are respectively used to design the total force along the flow direction and perpendicular to the relative motion. This result indicates that the bubbles are repelled from each other whatever the distance of separation. The DNS of Yuan & Prosperetti (1994) disagreed. It clearly demonstrated the existence of an equilibrium distance of separation for a tandem of bubbles moving in line. Considering the effect of the vorticity produced by the leading bubble and especially its transport and transverse diffusion in the wake (the latter mechanism being neglected in the first

https://doi.org/10.1017/S002211201000635X Published online by Cambridge University Press

work of Harper 1970), Harper (1997) calculated Moore's correction for two bubbles moving in line at the same velocity U_b:

$$C_{D1} = \frac{48}{Re}\left[1 - 2S^{-3} + \cdots - \frac{M_1}{Re^{1/2}}\right] - 12S^{-4} + \cdots, \tag{1.3}$$

$$C_{D2} = \frac{48}{Re}\left[1 - 2S^{-3} + \cdots - \frac{M_2}{Re^{1/2}}\right] + 12S^{-4} + \cdots, \tag{1.4}$$

where the Harper–Moore correction coefficients M_1 and M_2 depend on both the separating distance and the Reynolds number (note that in Harper 1970 $M_1 = M_\infty = 2.211$ and $M_2 = 4.345$). The dependence of M_1 is noticeable only at small distances so that in a first approximation $M_1 \approx 2.211$. The effect of the separating distance is more pronounced for M_2. Note that $M_2 \to 2.211$ as $d \to \infty$ for a fixed large Re and $M_2 \to 4.345$ as $Re \to \infty$ for a fixed large d, the latter case being of less practical use than the former. In all the situations, M_2 is found to be larger than M_1, so that the corresponding relative drag decrease can compensate the relative increase induced by the potential effect for a separating distance larger than a critical value d_e. In consequence, d_e is a stable equilibrium position that depends on the Reynolds number as shown by the DNS of Yuan & Prosperetti (1994). The existence of an equilibrium distance has not been observed in the experiments reported by Katz & Meneveau (1996). They reported the interaction in a chain of nearly spherical air bubbles rising in line at Reynolds numbers ranging from 0.2 to 140. They observed stable in-line bubble trajectories and a pairing-off process resulting in pair coalescence. This difference from the DNS of Yuan & Prosperetti (1994) and the analytical solution of Harper (1970, 1997) has been attributed to deformation and/or surfactants in several papers (see Bunner & Tryggvason 2003). According to Harper (1997, 2001), this pairing-off process, not predicted for two bubbles in line, does occur in the interaction of three or more bubbles both in the Stokes limit and at high Reynolds numbers.

The existence of an equilibrium distance has also been observed using DNS by Kim, Elghobashi & Sirignano (1993) for two rigid spheres translating side by side and by Legendre *et al.* (2003) for two bubbles in the same configuration. Legendre *et al.* (2003) clearly showed that for distances larger than an equilibrium distance d_e, the bubbles are attracted due to the Venturi effect in the separating gap between the bubbles as predicted by the potential theory. When the separating distance decreases, the vorticity produced on each bubble enters an interaction and generates a blocking effect for the flow in the gap, resulting in an increase in the pressure and the bubbles being repelled from each other. The numerical simulations also indicate that the drag of each bubble can be described by simply adding the Moore correction obtained for a single bubble with the potential viscous contribution:

$$C_{D1} = C_{D2} = \frac{48}{Re}\left[1 + S^{-3} - 3S^{-6}/4 + \cdots - \frac{M_\infty}{Re^{1/2}} + O(S^{-3}Re^{-1/2})\right], \tag{1.5}$$

while the transverse (or lift) force experienced by the bubbles when normalised as the drag force by $\pi R^2 \rho U_b^2/2$ can be written as

$$C_{L1} = -C_{L2} = 6S^{-4}\left[1 + S^{-3} + 16S^{-5}/3 + \cdots - \frac{40}{Re}\right]. \tag{1.6}$$

Using the definition of the present paper, a positive lift coefficient $C_{L1} > 0$ for the first (left) bubble combined with a negative lift coefficient $C_{L2} < 0$ for the second (right)

https://doi.org/10.1017/S002211201000635X Published online by Cambridge University Press

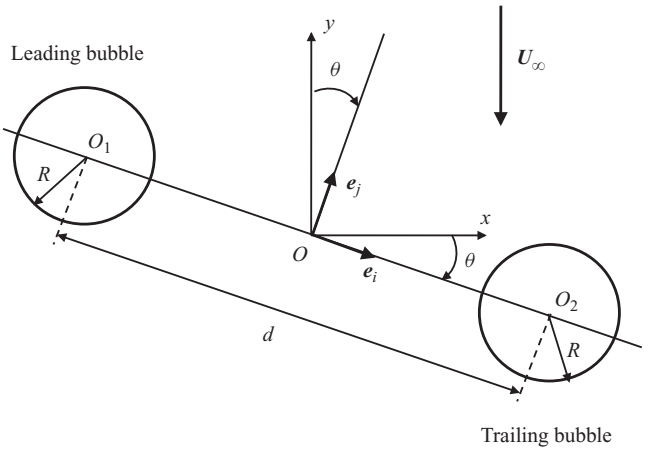


FIGURE 1. Sketch of the flow configuration and coordinate system.

bubble corresponds to the attraction between the bubbles. In (1.6), the potential effect $1 + L(S) = 1 + S^{-3} + 16S^{-5}/3 + \cdots$ (Kok 1993) is balanced by a viscous contribution ($\sim Re^{-1}$) of opposite sign that is responsible for the stable equilibrium position (Legendre *et al.* 2003).

The results reported above outline that the effect of the vorticity produced at the bubble surface and diffused and transported in its wake plays a crucial role in the mechanism of interaction for side-by-side and in-line bubbles. The objective of this work is to consider the general configuration for two bubbles rising in a liquid and to connect the results for the drag and lift coefficients obtained for the viscous potential flow condition, for two bubbles rising in line and two bubbles moving side by side.

2. Statement of the problem

We consider a pair of bubbles of radius R rising at the same velocity $U_b\boldsymbol{e}_y$ in a plane in an unbounded Newtonian fluid at rest. The Cartesian coordinates (x, y, z) associated with the Cartesian frame of reference $(\boldsymbol{e}_x, \boldsymbol{e}_y, \boldsymbol{e}_z)$ are defined in figure 1.

We also introduced the Cartesian frame $(\boldsymbol{e}_i, \boldsymbol{e}_j, \boldsymbol{e}_z)$ associated with the relative position of the two bubbles. Here $\boldsymbol{e}_i$ is directed along the axis joining the centres of the bubbles and directed from the left bubble called B1 to the right bubble called B2 (see figure 1), and $\boldsymbol{e}_j$ is normal to the centreline so that $\boldsymbol{e}_j \cdot \boldsymbol{e}_y > 0$. We define the origin O with coordinates (x_o, y_o, z_o) at mid-distance between the two bubbles and the bubbles' centres are located at O_1 (x_1, y_1, z_1) and O_2 (x_2, y_2, z_2), respectively. The distance of separation $d = O_1O_2$ between the two bubbles thus obeys $d^2 = (x_2 - x_1)^2 + (y_2 - y_1)^2 + (z_2 - z_1)^2$. These two frames enable us to define the angle θ characterising the relative position of the bubbles' centreline with respect to the $\boldsymbol{e}_x$-direction by $\theta = \arccos(\boldsymbol{e}_x \cdot \boldsymbol{e}_i) = \arccos(\boldsymbol{e}_y \cdot \boldsymbol{e}_j)$. For symmetry reasons, any configuration can be described with an angle ranging between $\theta = 0°$ (bubbles side by side) and $\theta = 90°$ (bubbles in line). In the $(O, \boldsymbol{e}_i, \boldsymbol{e}_j, \boldsymbol{e}_z)$ frame, the leading bubble is located at $-d/2\boldsymbol{e}_i$, the trailing bubble is located at $d/2\boldsymbol{e}_i$ and the flow at infinity is uniform $\boldsymbol{U}_\infty = -U_b\boldsymbol{e}_y$. We have checked by performing some three-dimensional simulations in the entire domain that, under the flow conditions studied here, the wake of the bubbles is not destabilised by the interaction, so the problem remains symmetric with respect to the plane $(O, \boldsymbol{e}_i, \boldsymbol{e}_j)$. Indeed, the induced effect of interaction is not

https://doi.org/10.1017/S002211201000635X Published online by Cambridge University Press

enough to generate the threshold value of vorticity at the bubble surface necessary for wake destabilisation (Magnaudet & Mougin 2007). Hence, the governing equations only need to be solved in one half of the space, say $z \geqslant 0$. Denoting the velocity and pressure fields by $\boldsymbol{V}$ and P, respectively, the incompressible flow surrounding the bubble pair is governed by the Navier–Stokes equations

$$\boldsymbol{\nabla} \cdot \boldsymbol{V} = 0, \tag{2.1}$$

$$\frac{\partial \boldsymbol{V}}{\partial t} + \boldsymbol{V} \cdot \boldsymbol{\nabla} \boldsymbol{V} = -\frac{1}{\rho} \boldsymbol{\nabla} P + \frac{1}{\rho} \boldsymbol{\nabla} \cdot \boldsymbol{\tau}, \tag{2.2}$$

where $\boldsymbol{\tau} = \mu(\boldsymbol{\nabla} \boldsymbol{V} + {}^{T}\boldsymbol{\nabla} \boldsymbol{V})$ is the viscous part of the stress tensor $\boldsymbol{\Sigma} = -P\boldsymbol{I} + \boldsymbol{\tau}$, ρ and μ being respectively the density and the dynamic viscosity of the liquid. The boundary condition far from the bubbles is

$$\boldsymbol{V} \to \boldsymbol{U}_{\infty} = -U_b \boldsymbol{e}_y \qquad \text{for } \boldsymbol{r} \to \infty, \tag{2.3}$$

where $r^2 = (x - x_o)^2 + (y - y_o)^2 + (z - z_o)^2$. Since there is no mass transfer through the interface of the bubbles, the normal velocity of the fluid must vanish on these surfaces. Moreover, the dynamic viscosity of the gas filling the bubbles is generally negligibly small compared with that of the surrounding liquid. In the absence of surfactants or contaminants on the bubble surface, the condition for the liquid at the interface is a shear-free condition due to the matching of the shear stresses across the bubble surfaces. Therefore, the boundary conditions at the interfaces are

$$\begin{cases} \boldsymbol{V} \cdot \boldsymbol{n} = 0 \\ \boldsymbol{n} \times (\boldsymbol{\tau} \cdot \boldsymbol{n}) = \boldsymbol{0} \end{cases} \qquad \text{on each bubble.} \tag{2.4}$$

The steady solution of this problem depends on three characteristic parameters, namely the Reynolds number Re, the non-dimensional distance S and the angle θ defined, respectively, as

$$Re = \frac{2R\rho U_{\infty}}{\mu}, \quad S = \frac{d}{R}, \quad \theta = \arccos(\boldsymbol{e}_x \cdot \boldsymbol{e}_i). \tag{2.5}$$

In each simulation reported in this paper, θ, Re and S are fixed and the converged values of the drag and lift forces are presented.

In the present study, the Reynolds number Re varies between 10 and 500, and the separation between the bubbles varies between $S = 2.5$ and 10 ($S = 2$ corresponds to bubbles in contact and $S = 3$ to bubbles separated by a gap of one radius). The angle θ varies between 0° and 90° with a denser distribution for high angles in order to improve the description of the interaction when the second bubble B2 is in the wake of the first bubble B1. We also assume that the bubbles remain spherical i.e. flow and fluid conditions correspond to Weber and Eötvös numbers, both small compared to unity. This study is mainly devoted to the understanding of the hydrodynamic interactions between the two bubbles. The forces acting on the leading bubble and the trailing bubble are $\boldsymbol{F_1}$ and $\boldsymbol{F_2}$, respectively. They are calculated by integrating the stress tensor on each bubble:

$$\boldsymbol{F_1} = \int_{\Gamma 1} \boldsymbol{\Sigma} \cdot \boldsymbol{n} \, \mathrm{d}\Gamma, \qquad \boldsymbol{F_2} = \int_{\Gamma 2} \boldsymbol{\Sigma} \cdot \boldsymbol{n} \, \mathrm{d}\Gamma, \tag{2.6}$$

where $\Gamma 1$ and $\Gamma 2$ denote the surfaces of bubbles B1 and B2, respectively. The dynamics can be studied using the components of these forces ($F_{L1}, -F_{D1}, F_{1z} = 0$) and ($F_{L2}, -F_{D2}, F_{2z} = 0$) in the Cartesian frame of reference ($\boldsymbol{e}_x, \boldsymbol{e}_y, \boldsymbol{e}_z$). As will be

https://doi.org/10.1017/S002211201000635X Published online by Cambridge University Press

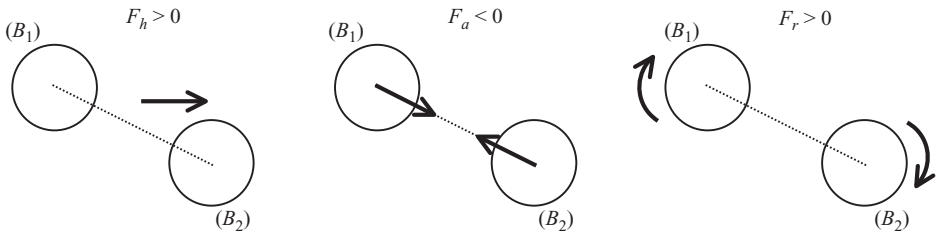


FIGURE 2. Interaction effect on bubble motion.

explained in the paper, we also introduce the following decomposition, which provides a better description of the interaction:

$$\left.\begin{aligned} F_v &= F_{D1} + F_{D2}, \\ F_h &= F_{L1} + F_{L2}, \\ F_r &= F_{1j} - F_{2j}, \\ F_a &= F_{2i} - F_{1i}, \end{aligned}\right\} \tag{2.7}$$

where $F_{2i} = F_{L2}\cos\theta + F_{D2}\sin\theta$, $F_{1i} = F_{L1}\cos\theta + F_{D1}\sin\theta$, $F_{2j} = F_{L2}\sin\theta - F_{D2}\cos\theta$ and $F_{1j} = F_{D1}\sin\theta + F_{L1}\cos\theta$ are respectively the $\boldsymbol{e}_i$- and $\boldsymbol{e}_j$-components of the forces $\boldsymbol{F}_1$ and $\boldsymbol{F}_2$. Note that F_v and F_h describe the $\boldsymbol{e}_x$- and $\boldsymbol{e}_y$-components acting on the system formed by the bubble pair and they point to the induced motion of its centre of mass O. By definition, the F_v component is positive. It will be compared with the drag force magnitude $F_{D\infty}$ acting on a single bubble under the same flow condition (same Re). If $F_v < 2F_{D\infty}$ (resp. $F_v > 2F_{D\infty}$), the centre of mass moves faster (resp. slower) than a single bubble. The effects of the three other components are summarised in figure 2. If $F_h > 0$, the centre of mass of the two bubbles drifts from the left to the right. The component F_a points to the relative attraction. If $F_a > 0$ (resp. $F_a < 0$), the two bubbles are repelled (resp. attracted). Finally, the component F_r gives information on the evolution of the relative orientation of the two bubbles. If $F_r > 0$, the bubbles rotate increasing the angle θ (evolution towards the in-line position), while for $F_r < 0$, the angle between the bubbles is decreased (evolution towards the side-by-side position).

All the force components introduced above are normalised by $\pi R^2 \rho U_\infty^2/2$ (resp. $\pi R^2 \rho U_\infty^2$) in order to define the dimensionless coefficients C_{D1}, C_{L1}, C_{D2} and C_{L2} (resp. C_v, C_h, C_r and C_a) associated with the force components F_{D1}, F_{L1}, F_{D2} and F_{L2} (resp. F_v, F_h, F_r and F_a). We also note $C_{D\infty} = F_{D\infty}/(\pi R^2 \rho U_\infty^2/2)$, the drag coefficient of a single isolated bubble in an unbounded situation. By definition, C_{D1}, C_{D2} and C_v tend to $C_{D\infty}$ and C_{L1}, C_{L2}, C_h, C_a and C_r vanish when $S \to \infty$. Knowing the value of the coefficients C_v, C_h, C_r and C_a, it is straightforward to calculate the drag and lift of each bubble:

$$\left.\begin{aligned} C_{D1} &= C_v - C_r\cos\theta - C_a\sin\theta, \\ C_{D2} &= C_v + C_r\cos\theta + C_a\sin\theta, \\ C_{L1} &= C_h + C_r\sin\theta - C_a\cos\theta, \\ C_{L2} &= C_h - C_r\sin\theta + C_a\cos\theta. \end{aligned}\right\} \tag{2.8}$$

3. Numerical procedure

The simulations presented below were carried out using the JADIM code described in previous works devoted to bubble dynamics studies (Magnaudet, Rivero & Fabre

https://doi.org/10.1017/S002211201000635X Published online by Cambridge University Press

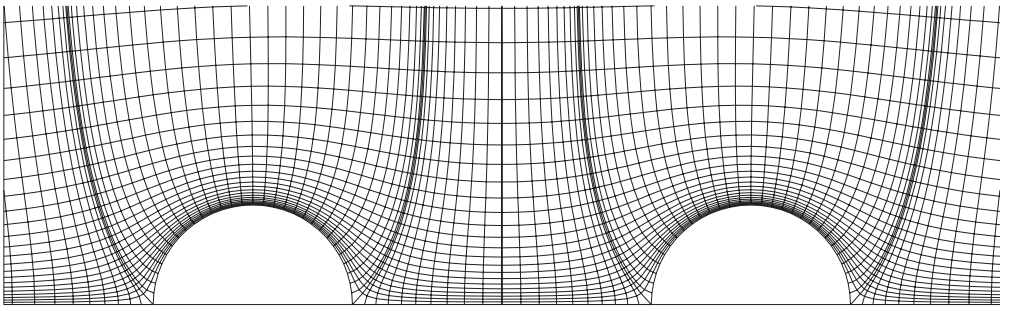


FIGURE 3. Partial view of the grid near the bubbles for $S = 5$.

1995; Legendre & Magnaudet 1998; Legendre *et al.* 2003; Merle, Legendre & Magnaudet 2005; Figueroa-Espinoza, Legendre & Zenit 2008). The reader is referred to Legendre *et al.* (2003), where the code is used to study the hydrodynamic interaction of two bubbles moving side by side. Briefly, the JADIM code solves the three-dimensional unsteady Navier–Stokes equations written in velocity–pressure variables in a general system of orthogonal curvilinear coordinates. The discretisation involves a staggered mesh and the equations are integrated in space using a finite volume method with second-order accuracy. All spatial derivatives are approximated using second-order centred schemes. The time advancement is realised through a Runge–Kutta/Crank–Nicolson algorithm which is second-order accurate in time, and incompressibility is satisfied at the end of each time step by using an auxiliary potential determined by solving a Poisson equation.

The grid used in this study is presented in detail by Legendre *et al.* (2003). The grid is based on a two-dimensional mesh obtained from the streamlines ($\eta = \text{const.}$) and equipotential lines ($\xi = \text{const.}$) of the potential flow generated by two circular cylinders moving in line along the ($\boldsymbol{e}_i$) axis. Then, the final three-dimensional grid is obtained by a rotation of the plane grid about the ($\boldsymbol{e}_i$) axis with an angle ϕ. An example of the grid is shown for $S = 5$ in figure 3.

Many numerical tests presented by Legendre *et al.* (2003) concerning the node distributions have been performed to prove that numerical results are grid-independent. Since these tests concern situations corresponding to $\theta = 0°$, we have performed additional tests in order to make sure that these grids can also be used for any value of θ between 0° and 90°. The same tests have been reproduced for the angle $\theta = 90°$ and especially $\theta = 45°$, corresponding to the more crucial situation in which the flow velocity observes most of the cells with an angle of 45°, which is known to be the worst situation for numerical accuracy. These tests have confirmed the choice of the numerical parameters for the grid presented in Legendre *et al.* (2003). Two examples are presented in tables 1 and 2. Table 1 reports numerical tests for the effect of the distance δ from the bubble surface to the first node above the surface, which is crucial for an accurate description of the interaction in the high-Reynolds-number regime (see Legendre *et al.* 2003). Table 2 reports the effect of the number of nodes N between the two bubbles. For all the simulations reported in this study, we have chosen $\delta/R = 0.002$ and $N = 20$ for $2.5 \leqslant S \leqslant 4.5$, $N = 30$ for $6 \leqslant S \leqslant 10$ and $N = 40$ for $S \geqslant 12$. Note that the same tests have been performed with the same conclusions for the potential results presented in the next section.

https://doi.org/10.1017/S002211201000635X Published online by Cambridge University Press

δ/R	C_v	C_h	C_a	C_r
0.001	0.112	0.0179	0.0224	0.109
0.002	0.111	0.0175	0.0222	0.110
0.004	0.111	0.0164	0.0217	0.112
0.01	0.108	0.0167	0.0240	0.115

TABLE 1. Effect of the relative size δ/R of the cell located on the bubble surface for $S=3$, $\theta=45^\circ$ and $Re=300$.

N	C_v	C_h	C_a	C_r
20	0.1111	0.01752	0.02218	0.1097
30	0.1112	0.01753	0.02221	0.1098
40	0.1112	0.01754	0.02222	0.1098

TABLE 2. Effect of the number of nodes between the two bubbles for $S=3$, $\theta=45^\circ$ and $Re=300$.

4. Additional numerical validations

4.1. *Interaction in irrotational flow*

Solutions for the force acting on two spheres of identical radius moving in an irrotational flow at an arbitrary angle with respect to their centrelines have been reported by Endo (1938) and by several other studies (Biesheuvel & van Wijngaarden 1982; Kok 1993). Following the global kinetic energy balance approach (Levich 1962), Kok (1993) evaluated the modification of the viscous drag force due to the hydrodynamic interaction between the two bubbles and proposed the forces acting on the bubbles in an irrotational viscous flow (given here up to $O(S^{-9})$ terms):

$$C_{v\,pot} = \frac{48}{Re}[1 + G^* + H^* \cos(2\theta)], \tag{4.1}$$

$$C_{h\,pot} = -\frac{48}{Re} H^* \sin(2\theta), \tag{4.2}$$

$$C_{a\,pot} = 2M^* - 2N^* \cos(2\theta), \tag{4.3}$$

$$C_{r\,pot} = 2L^* \sin(2\theta), \tag{4.4}$$

with

$$2G^* = -S^{-3} + \frac{15}{4}S^{-6} + 8S^{-8} - \frac{7}{2}S^{-9} + \cdots, \tag{4.5}$$

$$2H^* = 3S^{-3} - \frac{9}{4}S^{-6} - 4S^{-8} + \frac{9}{2}S^{-9} + \cdots, \tag{4.6}$$

$$2M^* = 3S^{-4} - 15S^{-7} - 64S^{-9} + \cdots, \tag{4.7}$$

$$2N^* = 9S^{-4} - 9S^{-7} - 32S^{-9} + \cdots, \tag{4.8}$$

$$2L^* = -6S^{-4} + 3S^{-7} + 8S^{-9} + \cdots. \tag{4.9}$$

It can be noted that the contributions C_v and C_h are zero in an inviscid flow. To check our code against these predictions, we considered the results obtained during the first time steps after the flow has been initialised with a uniform velocity profile far upstream. As vorticity is generated at the bubble surface by the shear-free condition and is then diffused in the boundary layer and shed in the wake, its influence is expected to be negligible during the very first time steps (typically over a period

https://doi.org/10.1017/S002211201000635X Published online by Cambridge University Press

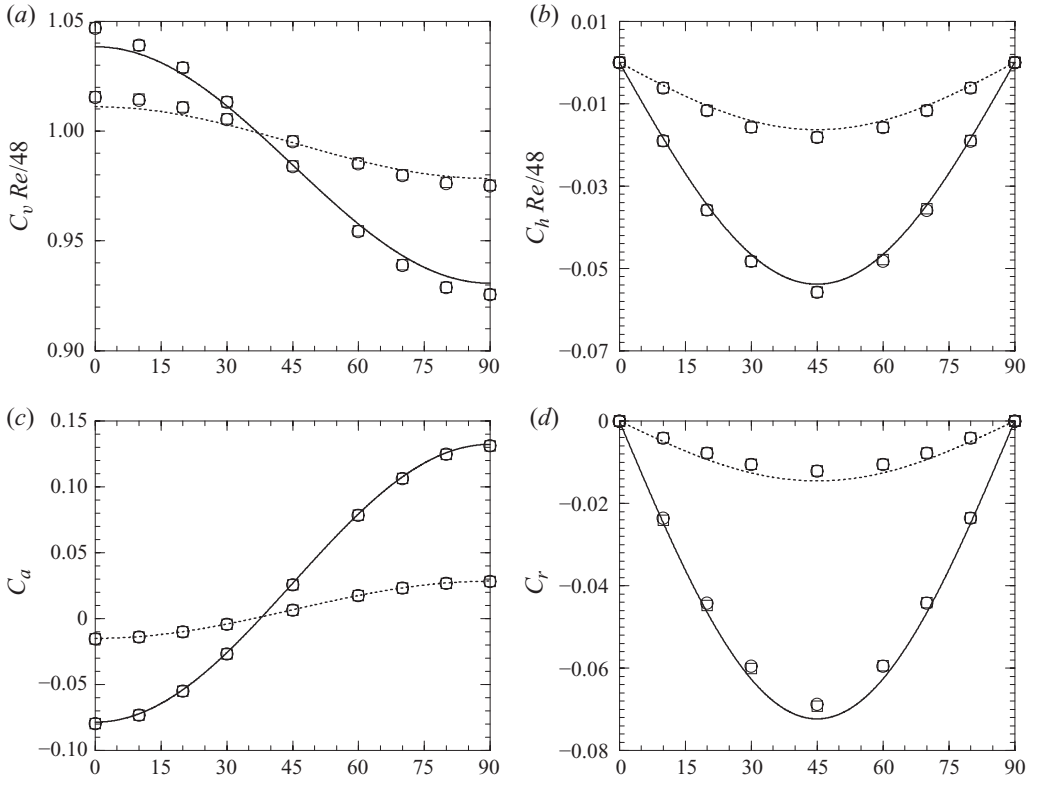


FIGURE 4. Potential simulations at (○) $Re = 20$ and (□) $Re = 200$. Dimensional coefficient (*a*) $C_v\,Re/48$, (*b*) $C_h\,Re/48$, (*c*) C_a and (*d*) C_r as a function of θ. Potential solution (4.1), (4.2), (4.3) and (4.4): —, $S = 3$; . . . , $S = 4.5$.

of time T such that $T \ll R^2/\nu$). Indeed, by choosing a very small time step Δt, we observed quasi-constant values of the coefficients over several tens of time steps. The results obtained for two different time steps $\Delta t = 10^{-6}R/U$ and $\Delta t = 10^{-5}R/U$ are very close. Figure 4 presents a comparison with the irrotational solution (4.1)–(4.4) at $Re = 20$ and $Re = 200$ for $S = 3$ and $S = 4.5$, respectively. These comparisons confirm the results presented by Legendre *et al.* (2003) for side-by-side bubbles concerning the ability of our code to properly capture the irrotational mechanisms of interaction.

4.2. *In-line bubbles* ($\theta = 90°$)

As discussed in the Introduction, the in-line interaction between two bubbles has been studied analytically and numerically (Yuan & Prosperetti 1994; Harper 1997). From the relation (4.1)–(4.4), it is possible to express the viscous potential solution for two bubbles moving in line as

$$C_{D1\,pot} = \frac{48}{Re}(1 + G^* - H^*) - 2M^* - 2N^*, \tag{4.10}$$

$$C_{D2\,pot} = \frac{48}{Re}(1 + G^* - H^*) + 2M^* + 2N^*. \tag{4.11}$$

The solution (1.3)–(1.4) is consistent with the first terms of the expansion reported in (4.10–4.11), since $2M^* + 2N^* = 12S^{-4} - 24S^{-7} - 96S^{-9} + \cdots$ and $G^* - H^* = -2S^{-3} + 3S^{-6} + 6S^{-8} + \cdots$. Our numerical simulations are compared with the analytical solution

https://doi.org/10.1017/S002211201000635X Published online by Cambridge University Press

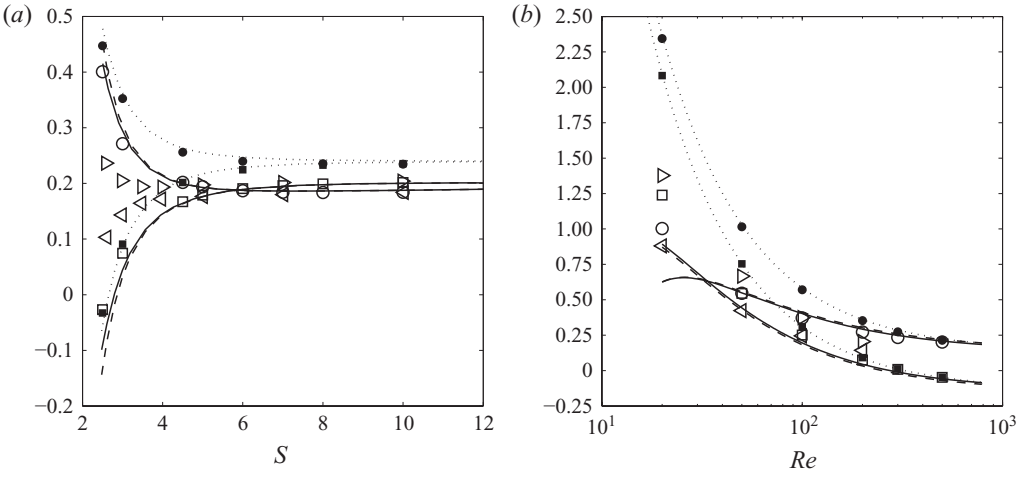


FIGURE 5. Evolution of the drag coefficient for two bubbles moving in line ($\theta = 90°$): (*a*) for $Re = 200$ and (*b*) for $S = 3$. Lines and symbols: ·····, potential solution (4.10)–(4.11); - - -, relations (1.3)–(1.4) from Harper (1997); —, relations (4.12)–(4.13). Numerical simulations: ○, C_{D1}; □, C_{D2}; ●, $C_{D1\,pot}$; ■, $C_{D2\,pot}$ (this study); ◁, C_{D1} and ▷, C_{D2} (Yuan & Prosperetti 1994; from their figure 2).

(1.3)–(1.4) and the DNS reported by Yuan & Prosperetti (1994). Figures 5(*a*) and 5(*b*) report a comparison at $S = 3$ for various Re and at $Re = 200$ for various S, respectively. Since for two bubbles moving side by side the drag evolution is very well described by simply adding the full potential solution and the Moore correction (Legendre *et al.* 2003), the results are also compared with the following expressions deduced from the potential solution (4.10)–(4.11) and the Moore correction derived by Harper (1997):

$$C_{D1} = \frac{48}{Re}\left(1 + G^* - H^* - \frac{M_1}{Re^{1/2}}\right) - 2M^* - 2N^*, \tag{4.12}$$

$$C_{D2} = \frac{48}{Re}\left(1 + G^* - H^* - \frac{M_2}{Re^{1/2}}\right) + 2M^* + 2N^*. \tag{4.13}$$

Figure 5(*a*) shows that for $Re = 200$ our results are in good agreement with expressions (4.12)–(4.13) and (1.3)–(1.4) for all the separating distances covered by the study. Note that the difference between (4.12)–(4.13) and (1.3)–(1.4) is very small since it is proportional to terms of order $O(S^{-7}, Re^{-1}S^{-6})$. The agreement with the simulations of Yuan & Prosperetti (1994) is very good for $Re = 200$ if $S > 4$. Figure 5(*b*) indicates that for $S = 3$ the agreement is satisfactory with relations (4.12)–(4.13) for $Re \geqslant 100$. For $S = 3$, the agreement with Yuan & Prosperetti (1994) is very good for $Re = 100$, acceptable for $Re = 200$ and not satisfactory for $Re = 20$ and $Re = 50$. The main reason could be attributed to the grid used in both studies, especially in the gap between the bubbles, which is crucial when the distance between the two bubbles is small (Legendre *et al.* 2003). To check the origin of the discrepancy, additional simulations to prove grid independence of our results were performed. We have tested the effect of (i) the distance δ from the bubble surface to the first node (table 3*a*), (ii) the number of nodes N between the two bubbles (table 3*b*) and (iii) the number of nodes N_b used to describe the bubble surfaces (table 3*c*). These tests confirm that our results are grid-independent for the case of two bubbles moving

https://doi.org/10.1017/S002211201000635X Published online by Cambridge University Press

(a)			(b)			(c)		
δ/R	C_{D1}	C_{D2}	N	C_{D1}	C_{D2}	N_b	C_{D1}	C_{D2}
0.001	0.0745	0.272	10	0.744	0.272	20	0.0773	0.272
0.002	0.0745	0.272	20	0.745	0.272	30	0.0745	0.272
0.004	0.0744	0.271	30	0.745	0.272	40	0.0735	0.272
0.01	0.0743	0.270	40	0.745	0.272			

TABLE 3. Effect of the grid parameter for two bubbles moving in line ($\theta = 90°$) at $S = 3$ and $Re = 200$. (a) Effect of the relative size δ/R of the first cell located on the bubble surface for $N = 20$ and $N_b = 30$. (b) Effect of the number of nodes N between the bubbles for $\delta/R = 0.002$ and $N_b = 30$. (c) Effect of the number of nodes N_b on the bubble surface for $\delta/R = 0.002$ and $N = 20$.

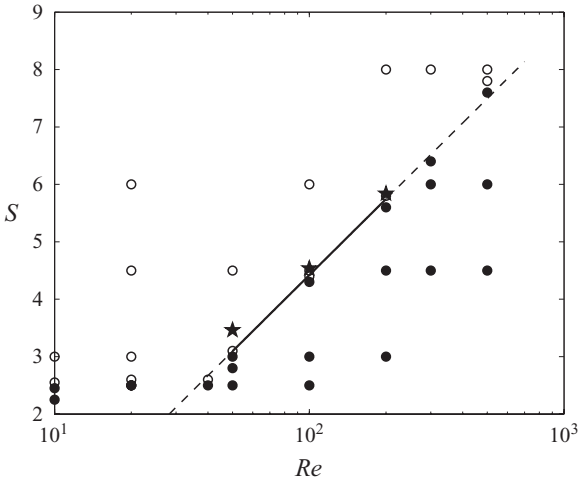


FIGURE 6. Equilibrium distance between two bubbles moving in line. Symbols: ○, attracted bubbles; ●, repelled bubbles (this study); —, relation (4.14) for $50 < Re < 200$ (Yuan & Prosperetti 1994); — — —, relation (4.14) $30 < Re < 500$; ★, solution of (4.16).

in line. Following the procedure presented in the previous section, we have also done additional simulations for $\theta = 90°$, which confirms that the potential effect is properly reproduced up to smaller separation distances. The comparison is reported for $Re = 200$ and $S = 3$ using black symbols in figures 5(a) and 5(b), respectively.

The equilibrium distances $S_e = d_e/R$ deduced from our simulations are reported in figure 6 and compared with the relation

$$S_e = 4.40 \log Re - 4.38, \tag{4.14}$$

deduced by Yuan & Prosperetti (1994) from their numerical simulations for $50 < Re < 200$. The equilibrium distance is found to be in very good agreement between the two numerical studies in the range covered by Yuan & Prosperetti (1994). Our simulations show that this correlation can be extended to larger Reynolds numbers but it cannot predict the asymptotic behaviour in the limit of lower Reynolds numbers, since the separating distance seems to evolve as

$$S_e \to 2 \quad \text{when } Re \to O(1). \tag{4.15}$$

https://doi.org/10.1017/S002211201000635X Published online by Cambridge University Press

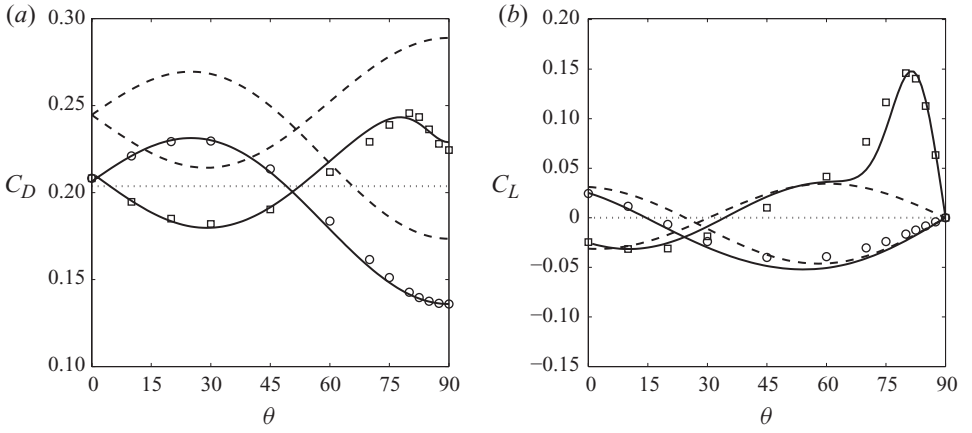


FIGURE 7. Drag and lift coefficients at $Re = 200$ and $S = 3.75$ versus θ (in-line bubbles for $\theta = 90°$ and side-by-side bubbles for $\theta = 0°$): (*a*) C_D and (*b*) C_L. Lines and symbols: ○, leading bubble B1; □, trailing bubble B2; – – –, potential solution; —, expressions (6.3), (6.6), (6.7) and (6.12) for C_{D1}, C_{L1}, C_{D2} and C_{L2}; . . . , drag and lift coefficients for a single bubble in an unbounded fluid.

This limit is in agreement with the Stokes flow solution, since it can be deduced from the solution for two solid spheres (Happel & Brenner 1965) that two bubbles moving in line are attracted at low but non-zero Reynolds number. Indeed, using analytical arguments first presented in Legendre & Magnaudet (1997), the drag expression for two solid spheres moving in line can be extended to bubbles using the prefactor (2/3).

From expression (4.12)–(4.13), the equilibrium distance S_e is reached when $C_{D1} = C_{D2}$:

$$12\,(M_2 - M_1) = Re^{3/2}(M^* + N^*). \tag{4.16}$$

Since M_2 and M_1 are both complex functions of Re and S (see Harper 1997), the equilibrium distance S_e for a given Reynolds number or the equilibrium Reynolds number Re_e for a given distance are determined from (4.16) using an iterative procedure. The corresponding equilibrium distance S_e is thus reported for comparison in figure 6 for $Re =$ 50, 100 and 200 using black stars. The agreement is very good for $Re > 100$, which confirms the range of validity of relation (1.3).

5. Description of the interaction between the two bubbles

The hydrodynamic interaction between the two bubbles is first mentioned for $Re = 200$ and $S = 3.75$. The drag coefficients C_{D1}, C_{D2} and lift coefficients C_{L1}, C_{L2} are reported in figure 7 versus the orientation angle θ. These coefficients are compared with the potential solution deduced from (4.1)–(4.4). We observe that the evolution of the drag coefficients seems to be deduced from the potential solution by a simple translation except for C_{D2} when $\theta \gtrsim 75°$. For the lift coefficient, the evolution is close to the potential one except for C_{L2} when $\theta \gtrsim 75°$. This specific change of behaviour for both the drag and the lift of the second bubble is due to the interaction with the wake of the first bubble. Note that C_{D1} and C_{D2} are compared with the drag coefficient $C_{D\infty}$ experienced by a single bubble moving in an unbounded fluid at the same Reynolds number. When the bubbles are side by side ($\theta = 0°$), they experience a drag which is slightly higher than that of a single bubble. When θ increases, the

https://doi.org/10.1017/S002211201000635X Published online by Cambridge University Press

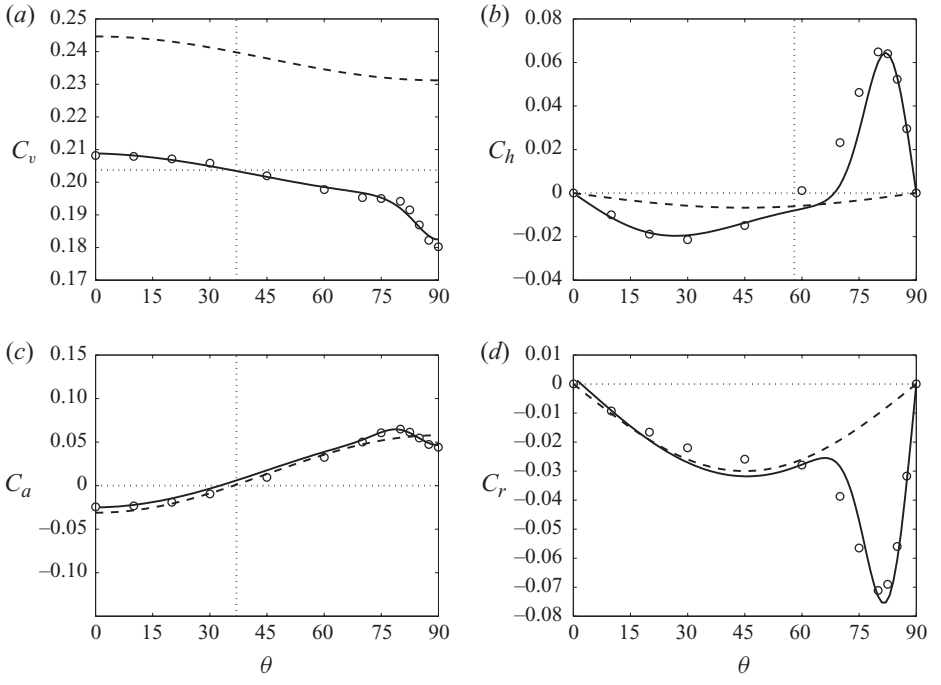


FIGURE 8. (*a–d*) Coefficients C_v, C_h, C_a and C_r for $Re = 200$ and $S = 3.75$. Lines: — — —, potential solution; —, evolutions deduced from expressions (6.3), (6.6), (6.7) and (6.12); . . . , drag and lift coefficients for a single bubble in an unbounded fluid. Vertical dashed lines show $\theta_v = 37°$, $\theta_h = 58°$ and $\theta_a = 37°$, respectively.

drag of the first (left) bubble first starts to increase while the drag of the second (right) bubble decreases, so that $C_{D1} > C_{D2}$ for $\theta \lesssim 53°$. This means that the bubbles are attracted along the $\boldsymbol{e}_y$-direction. For $\theta \lesssim 28°$, the lift coefficient of the first bubble is larger than that of the second bubble, $C_{L1} > C_{L2}$, corresponding to an attraction along the $\boldsymbol{e}_x$-direction. The combination of the simultaneous attraction along the $\boldsymbol{e}_x$- and $\boldsymbol{e}_y$-directions indicates that the two bubbles are attracted for $\theta \lesssim 28°$. The drag difference between the two bubbles is maximum for $\theta \sim 30°$ and is then reduced. The two bubbles again experience the same drag for $\theta \sim 53°$, which is nearly the drag of a single bubble. For $\theta \gtrsim 53°$, $C_{D1} < C_{D2}$ and $C_{L1} < C_{L2}$, so that the bubbles are repelled. The behaviour is similar to the one observed in potential flow where the bubbles are attracted for $0 < \theta < \theta_a$ and repelled for $\theta_a < \theta < 90°$, as presented in the Introduction (Kok 1993). This classic force decomposition (drag and lift) does not allow the value of θ_a to be known, i.e. whether the bubbles are attracted for $28° \lesssim \theta \lesssim 53°$ or not.

In order to make precise the angle of transition θ_a between attraction and repulsion as well as the direction of the torque acting on the tandem, we use the force decomposition introduced in § 2. The four coefficients C_v, C_h, C_a and C_r are plotted in figure 8 for $Re = 200$ and $S = 3.75$. The plot of the attraction coefficient C_a indicates that $\theta_a \sim 37°$, the two bubbles being attracted ($C_a \leqslant 0$) for $0 < \theta \leqslant \theta_a$ but repelled for $\theta_a \leqslant \theta < 90°$. The plot of the coefficients C_v and C_h also reveals two other critical angles $\theta_v \sim \theta_a \sim 37°$ and $\theta_h \sim 58°$. Indeed, the centre of inertia of the tandem moves slower than a single bubble ($C_v \geqslant C_{D\infty}$) for $0 < \theta \leqslant \theta_v$, while it moves faster for larger angles. The bubble tandem drifts from the right to the left ($C_h \leqslant 0$) for $0 \leqslant \theta \leqslant \theta_h$. For larger angles, the drift changes direction. The coefficient C_h reaches a maximum for

https://doi.org/10.1017/S002211201000635X Published online by Cambridge University Press

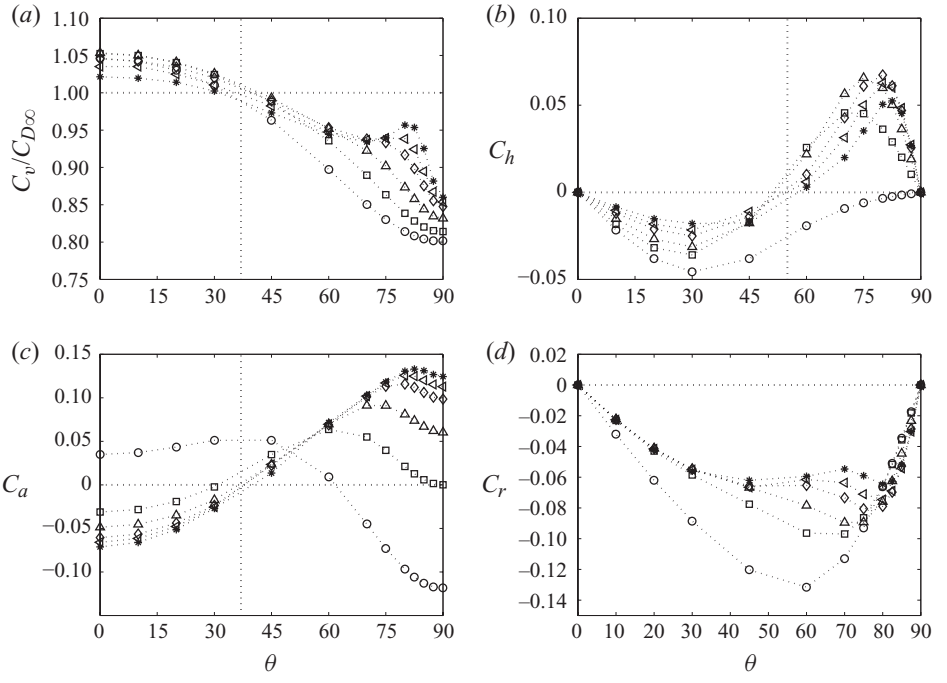


FIGURE 9. (*a–d*) Effect of the Reynolds number on the coefficients $C_v/C_{D\infty}$, C_h, C_a and C_r for $S=3$. Symbols: $*$, $Re=500$; $\triangleleft$, $Re=300$; $\diamond$, $Re=200$; $\triangle$, $Re=100$; $\square$, $Re=50$; $\circ$, $Re=20$. Vertical dashed lines show $\theta_v=37°$, $\theta_h=55°$ and $\theta_a=37°$, respectively.

$\theta_{max}\sim 80°$. Finally, the rotation coefficient C_r is negative for all the angles, showing a torque action on the tandem that tends to organise the bubbles side by side. Thus, for $Re=200$ and $S=3.75$, the in-line motion is unstable while the side-by-side position is stable. The maximum torque is also observed at $\theta=\theta_{max}\sim 80°$, indicating a similar origin for both behaviours. The significant change observed for the drag and lift of the trailing bubble for $\theta\gtrsim 75°$ is also very clear for the four interaction coefficients.

Using these four non-dimensional coefficients, the Reynolds number effect on bubble interaction is shown for $S=3$ in figure 9. To make the comparison between different Reynolds numbers easier, the coefficient C_v is normalised by the drag coefficient of a single bubble $C_{D\infty}$. Note that $C_v/C_{D\infty}$ is found to have a similar evolution for the different Reynolds numbers until the second bubble enters in the wake of the first bubble. The corresponding drag decrease is then significantly dependent on the Reynolds number because the velocity wake decay depends on Re as shown in the Appendix. The plot shows that the critical angle $\theta_v\sim 37°$ is found to be nearly independent of the Reynolds number for $S=3$.

Concerning the $\boldsymbol{e}_x$- or drift coefficient C_h, the same evolution is observed with a change of drift direction at a nearly constant angle $\theta_h\sim 55°$ except at $Re=20$. At this Reynolds number, $C_h<0$ for all the angles. We also observe that for $\theta<\theta_h$, the magnitude of the drift force of the tandem decreases when increasing the Reynolds number, in agreement with the potential solution. After the change of drift direction, we observe that the combined influence of the potential contribution and the wake of the first bubble makes the behaviour more complex.

For $Re>50$, the evolution of the attractive coefficient C_a with the angle looks similar whatever the Reynolds number, so that θ_a is nearly independent of Re: the

https://doi.org/10.1017/S0022112010006635X Published online by Cambridge University Press

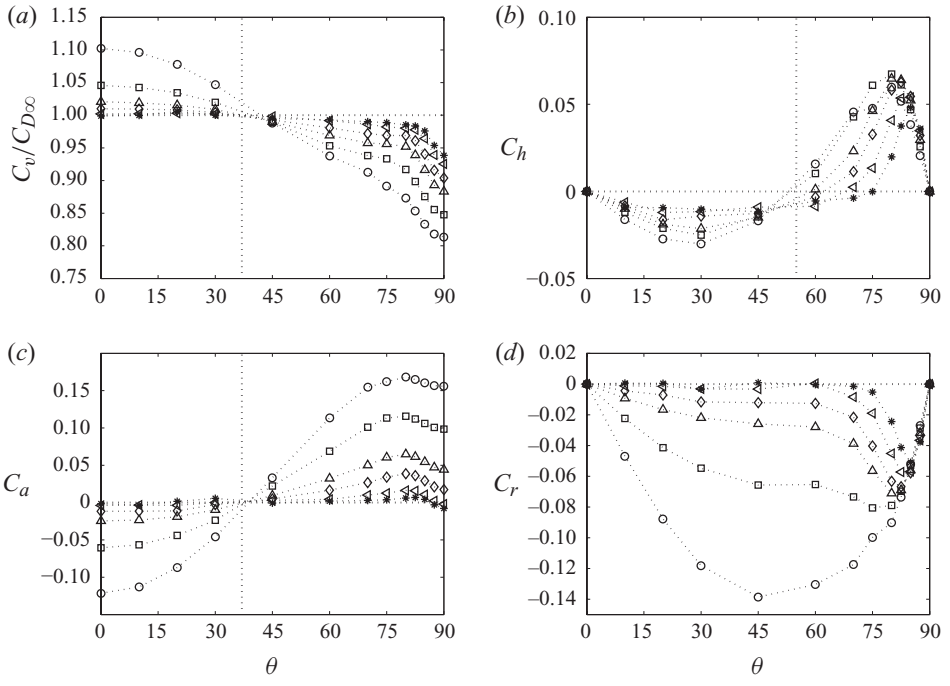


FIGURE 10. (a–d) Effect of the separating distance S on the coefficients $C_v/C_{D\infty}$, $C\hat{h}$, C_a and C_r for $Re = 200$. Symbols: ○, $S = 2.5$; □, $S = 3$; △, $S = 3.75$; ◇, $S = 4.5$; ◁, $S = 6$; ∗, $S = 8$. Vertical dashed lines show $\theta_v = 37°$, $\theta_h = 55°$ and $\theta_a = 37°$, respectively.

bubbles are attracted for $0 < \theta < \theta_a$ and repelled for larger angles. We have $\theta_a \sim 37°$ from figure 9. As observed for C_v and C_h, a noticeable change of behaviour is observed when the trailing bubble interacts with the wake of the leading bubble. The region of wake influence increases when Re decreases due to a stronger diffusion of the wake at lower Reynolds numbers. Completely different behaviour is observed for $Re = 20$. Indeed, it can be noticed that for $Re = 20$ and $S = 3$, the sign of C_a is the opposite of that for larger Reynolds numbers: for $0 < \theta < 60°$, the two bubbles are repelled, but attracted for $60° < \theta < 90°$. This is in agreement with figure 6, where the equilibrium distance for $\theta = 0°$ is $S_e(Re = 20) \sim 2.6 < 3$.

Concerning the rotation coefficient, figure 9 clearly shows that C_r is negative whatever the Reynolds number, indicating that the side-by-side configuration is the only stable position. For $Re > 50$, the magnitude of the torque is found to be independent of the Reynolds number for $0 < \theta < 40°$ and close to the potential value (see figure 8). Again, when the second bubble is influenced by the wake of the first bubble, C_r is significantly influenced by the Reynolds number.

The effect of the separating distance is reported in figure 10 at $Re = 200$. The same trend is observed for the four coefficients, but their magnitude is significantly influenced by the separation. Obviously, the magnitude of the interaction becomes stronger when the separation decreases. For $S = 6$ and $S = 8$, only the wake effect seems to contribute towards bubble interaction. We also observe that the critical angles θ_a, θ_v and θ_h are nearly independent of the separation for $Re = 200$.

The description of both the effect of the Reynolds number and separation distance has been presented in this section. We have shown that the interaction can be characterised by three critical angles that are nearly constant for $Re \geqslant 50$ and for

https://doi.org/10.1017/S002211201000635X Published online by Cambridge University Press

the separation considered here ($2.5 \leqslant S \leqslant 10$). The bubbles are attracted for $0 < \theta < \theta_a$ with $\theta_a \sim 37^\circ$ and repelled for larger angles; the tandem experiences a drag larger than that of a single bubble for $0 < \theta < \theta_v$ with $\theta_v \sim \theta_a \sim 37^\circ$, the drag C_v being lower for larger angles; the centre of inertia drifts from the right to the left ($C_h < 0$) for $0 < \theta < \theta_h$. The critical angle θ_h is significantly affected by the separating distance. The torque applied on the system always has the same effect whatever S and Re, and tends to form the side-by-side configuration. It is also clear that the wake of the leading bubble induces a significant effect compared with what the potential flow solution describes. This particular wake effect is analysed in detail in the next section. For this purpose, the characterisation of the wake of a single bubble is reported in the Appendix. The velocity is described in the near wake and a simple model based on the far-wake velocity profile is proposed.

6. Drag and lift forces

The aim of this section is to propose simple expressions based on physical arguments to describe the forces experienced by each bubble. The discussion is conducted using the drag and lift coefficients. The corresponding expression for the coefficients C_v, C_h, C_a and C_r can be directly obtained using relations (2.7), and are shown for comparison with numerical results in figure 8.

6.1. *Leading bubble*

In the side-by-side configuration, Legendre *et al.* (2003) showed that the drag of the bubbles can be satisfactorily described by simply superposing the potential viscous drag and the Moore correction. Expression (1.5) can also be written as

$$C_{D1}(\theta = 0^\circ) = C_{D1\,pot} - M_\infty \frac{48}{Re^{3/2}}(1 + S^{-3}), \tag{6.1}$$

where $C_{D1\,pot}$ is given by (4.10). In the in-line configuration, we have shown in § 4.2 that the drag coefficient of the leading bubble can be expressed as

$$C_{D1}(\theta = 90^\circ) = C_{D1\,pot} - M_1 \frac{48}{Re^{3/2}}, \tag{6.2}$$

where a good approximation consists in considering $M_1 \simeq M_\infty = 2.211$ (Yuan & Prosperetti 1994; Harper 1997). Considering these two expressions, it is therefore attractive to propose the following very simple relation for any tilt angle:

$$C_{D1} = C_{D1\,pot} - M_\infty \frac{48}{Re^{3/2}}(1 + S^{-3}\cos\theta). \tag{6.3}$$

This model is found to describe correctly the simulations for $Re \geqslant 50$. An example of comparison is reported in figure 7. Consequently, the main difference between the potential solution and the simulations for C_{D1} is due to the Moore correction. It can be noticed that a small discrepancy is observed for very small separations and $\theta \simeq 90^\circ$ when using $M_1 \simeq M_\infty = 2.211$, since this value is slightly lower than the analytical value (Harper 1997). The agreement is improved if the value of M_1 obtained by Harper (1997) is used in (6.3). Note that the S^{-3} correction is a small contribution to the total drag coefficient.

In the side-by-side configuration, Legendre *et al.* (2003) found the lift coefficient to be given by (1.6). This expression is also written as

$$C_{L1}(\theta = 0^\circ) = C_{L1\,pot} - \frac{240}{ReS^4}, \tag{6.4}$$

https://doi.org/10.1017/S002211201000635X Published online by Cambridge University Press

where $C_{L1\,pot}$ is given by (2.8), (4.2) and (4.3). In the in-line case, the two bubbles experience no lift force, so that

$$C_{L1}(\theta = 90^\circ) = 0. \tag{6.5}$$

A simple extension of these two limit relations is to propose the following expression for the lift coefficient experienced by the first bubble:

$$C_{L1} = C_{L1\,pot} - \frac{240}{ReS^4} f_1(\theta), \tag{6.6}$$

where $f_1(\theta)$ is a function that satisfies $f_1(90^\circ) = 0$ and $f_1(0^\circ) = 1$. The expression $f_1(\theta) = \cos\theta[1 - (1 - 0.00053ReS^3)\sin(2\theta)\cos^3(\theta)]$ makes possible the description of the numerical values for any tilt angle. This relation is reported for comparison in figure 7, where the agreement with numerical data is very good.

6.2. *Trailing bubble*

As shown before, the effect of interaction is more pronounced on the trailing bubble when it enters an interaction with the wake of the first bubble. The objective is again to connect the drag force expression when the two bubbles are rising side by side (1.5) and when they are moving in line (4.12). For this purpose, we propose writing the drag coefficient as

$$C_{D2} = C_{D2\,pot} - 48\frac{M_2^*}{Re^{3/2}}, \tag{6.7}$$

where $M_2^* \to M_\infty$ when $\theta \to 0^\circ$ and $M_2^* \to M_2$ when $\theta \to 90^\circ$. The objective is to correctly reproduce the induced wake effect on the Moore correction. This effect is maximum when the bubbles are in line and vanishes when the second bubble is not influenced by the wake of the first bubble. The idea is to introduce in the Moore term a correction based on the wake characteristics as

$$M_2^* = M_\infty F(\tilde{u}_{rot}), \tag{6.8}$$

where $\tilde{u}_{rot}$ is the rotational part of the wake of a single bubble given by (A 4) in the Appendix, with $\tilde{X} = S\sin\theta$ and $\tilde{Y} = S\cos\theta$. An inspection of our results reveals that the expression

$$F(\tilde{u}_{rot}) = \left(1 - \frac{\alpha_2}{\alpha}\tilde{u}_{rot}\right)^{-3/2}, \tag{6.9}$$

with $\alpha_2 = (0.085S + 0.124)$, makes possible a very satisfactory description of the drag decrease of the trailing bubble when located in the wake of the first bubble, as shown in figure 7. The comparison is reported in figures 11 and 12 for ($Re = 200$, $S \in [2.5; 8]$) and ($Re \in [20; 500]$, $S = 3$), respectively. This result indicates that the induced wake effect is correctly described using a Moore correction by considering a modified Reynolds number $2R\rho U_\infty(1 - \tilde{u})/\mu$ based on the rotational part of the wake $\tilde{u} = \alpha_2/\alpha\tilde{u}_{rot}$ seen by the trailing bubble. Thus, the wake velocity defect needs to be corrected by α_2/α since the second bubble is not completely embedded into the wake of the first bubble and the velocity is not uniform at the bubble scale. The wake width is thinner than the bubble size when close to the first bubble and larger when located far downstream. In addition, the width of the wake depends on the Reynolds number, as shown in the Appendix.

As observed in figure 7, the second bubble experiences a significant transverse or lift force when interacting with the wake of the first bubble. Out of the wake, the lift effect can be described by simply superposing the potential contribution and a

https://doi.org/10.1017/S002211201000635X Published online by Cambridge University Press

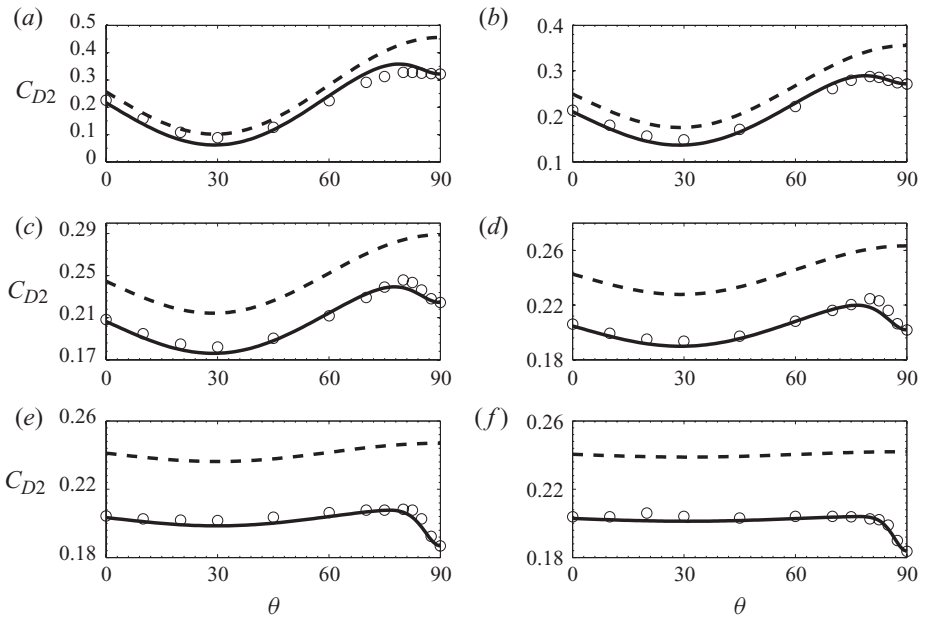


FIGURE 11. Drag coefficient C_{D2} of the trailing bubble at $Re = 200$. (*a*) $S = 2.5$, (*b*) $S = 3$, (*c*) $S = 3.75$, (*d*) $S = 4.5$, (*e*) $S = 6$ and (*f*) $S = 8$. Symbols: ○, numerical results; - - -, analytical potential drag; ——, relation (6.7).

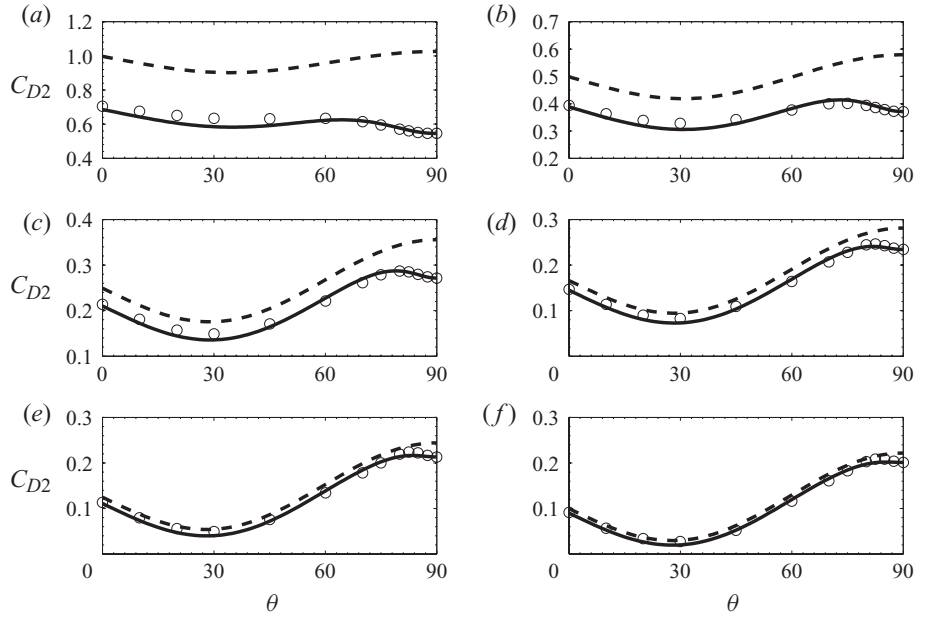


FIGURE 12. Drag coefficient C_{D2} of the trailing bubble at $S = 3$. (*a*) $Re = 20$, (*b*) $Re = 50$, (*c*) $Re = 100$, (*d*) $Re = 300$, (*e*) $Re = 400$ and (*f*) $Re = 500$. Symbols: ○, numerical results; - - -, analytical potential drag; ——, relation (6.7).

viscous correction of the form $240S^{-4}Re^{-1}f_2(\theta)$, as done for the leading bubble with $f_2(\theta) = \cos\theta[1 + (1 - 0.00053ReS^3)\sin(2\theta)\cos^3(\theta)]$. The combined contributions of C_{L1} and C_{L2} make possible a good description of the transverse motion of the bubble

https://doi.org/10.1017/S002211201000635X Published online by Cambridge University Press

pair as shown in figure 8 by the evolution of $C_h = (C_{L1} + C_{L2})/2$ for $0 < \theta < 40^\circ$. In the wake, the direction of the additional wake effect is in agreement with the classical lift force experienced by an isolated spherical bubble in a uniform unbounded linear shear flow (Auton 1987; Legendre & Magnaudet 1998):

$$\boldsymbol{F}_L = C_L \frac{4\pi R^3}{3} \rho(\boldsymbol{u} - \boldsymbol{v}) \times (\nabla \times \boldsymbol{u}), \tag{6.10}$$

where $\boldsymbol{v}$ is the velocity of the bubble, $\boldsymbol{u}$ is the unperturbated flow evaluated at the centre of the bubble and C_L is the lift coefficient. For a perfect fluid, Auton (1987) showed that $C_L^A = 1/2$ in the limit of weak shear flow. Legendre & Magnaudet (1998) extended this result to viscous fluid and moderate shear rate and proposed the relation $C_L^{LM} = C_L^A(Re + 16)/(Re + 29)$ to describe the lift coefficient for $Re \geqslant 5$. The lift coefficient is found to be lower than 1/2 for moderate Reynolds numbers.

In the frame of reference fixed with the bubbles, one has $\boldsymbol{u} = -U_\infty(1 - \tilde{u}_{wake})\boldsymbol{e}_y$ and $\boldsymbol{v} = 0$, so that using relation (A 4) the corresponding lift effect is

$$\boldsymbol{F}_L = C_L \frac{\pi R^3}{3} \rho U_\infty^2 \beta Re \frac{\tilde{Y}}{\tilde{X}} (1 - \tilde{u}_{wake}) \tilde{u}_{rot} \boldsymbol{e}_x, \tag{6.11}$$

with $\tilde{X} = S \sin\theta$ and $\tilde{Y} = S \cos\theta$. The total transverse lift coefficient is then given by

$$C_{L2} = C_{L2\,pot} + \frac{240}{ReS^4} f_2(\theta) + \frac{2}{3} C_{L\,wake} \beta Re \frac{\cos\theta}{\sin\theta} (1 - \tilde{u}_{wake}) \tilde{u}_{rot}. \tag{6.12}$$

Note that the wake contribution to C_{L2} vanishes for a given separating distance when $\theta \to 0$. The lift coefficient is reported in figures 13 and 14 for various Reynolds numbers and separations (see also figure 7). The transverse effect is shown to be satisfactorily reproduced by relation (6.12). In particular, it is possible to correctly describe the location of the peak of lift in the wake as well as the region of the wake influence (see also C_h and C_r in figure 8). This additional transverse wake effect can clearly be attributed to a shear-induced lift force. The corresponding shear-induced lift coefficient $C_{L\,wake}$ varies between 0.05 and 0.35. The lift coefficient is found to depend on both the distance between the two bubbles and their Reynolds number. This can be attributed to the wake characteristics: the width of the rotational region increases with the distance to the bubble while the magnitude of the vorticity decreases. In addition, the second bubble cannot be considered as embedded in an unbounded linear shear flow since the lift effect is induced by a vorticity region corresponding to the wake of the first bubble. The corresponding wake width is thinner than the bubble size when close to the first bubble and larger when located far downstream. At a given position (fixed S), the width of the wake also decreases when the Reynolds number increases. The local size of the wake δ_w can be characterised by twice the distance from the axis where the velocity is half of the axis velocity. From the velocity profile in the wake given by (A 4), one has

$$\frac{\delta_w^2}{R^2} = 32 \ln(2) \frac{S}{\beta Re}, \tag{6.13}$$

where β is calculated by considering that $\tilde{X} \sim S$ in the bubble wake. Figure 15 reports the evolution of $C_{L\,wake}$ as a function of δ_w/R. This plot clearly shows that the induced lift effect strongly depends on the relative size between the wake (that contains the vorticity of the flow) and the bubble. We observe that $C_{L\,wake}$ increases with δ_w/R with values lower than $C_L^A = 1/2$, while $C_{L\,wake}$ decreases to zero as the relative size of the wake decreases. Figure 15 also reveals that the induced shear lift force remains

https://doi.org/10.1017/S002211201000635X Published online by Cambridge University Press

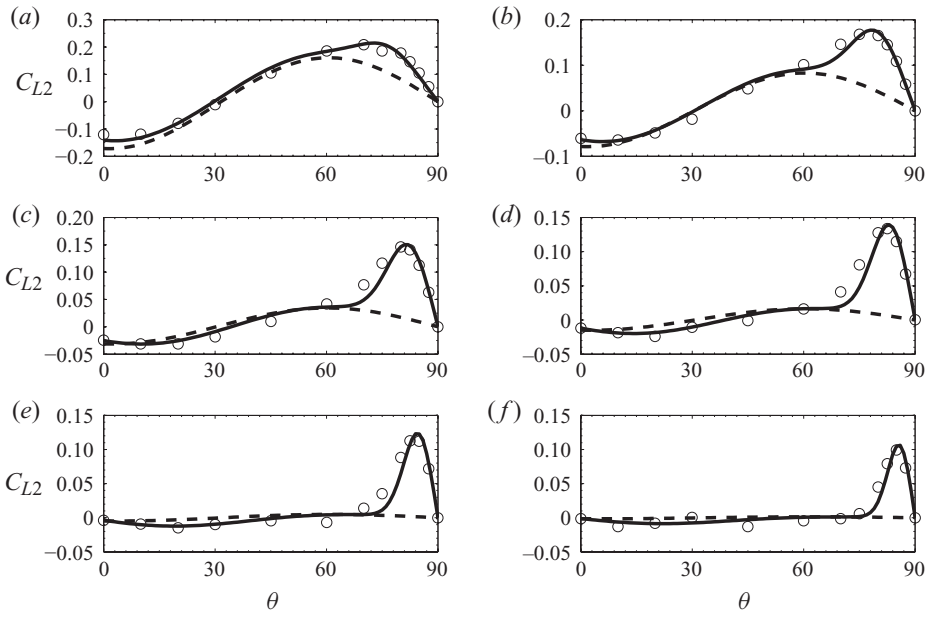


FIGURE 13. Lift coefficient C_{L2} of the trailing bubble at $Re = 200$. (*a*) $S = 2.5$, (*b*) $S = 3$, (*c*) $S = 3.75$, (*d*) $S = 4.5$, (*e*) $S = 6$ and (*f*) $S = 8$. Symbols: ○, numerical results; - - -, analytical potential lift; ——, relation (6.12).

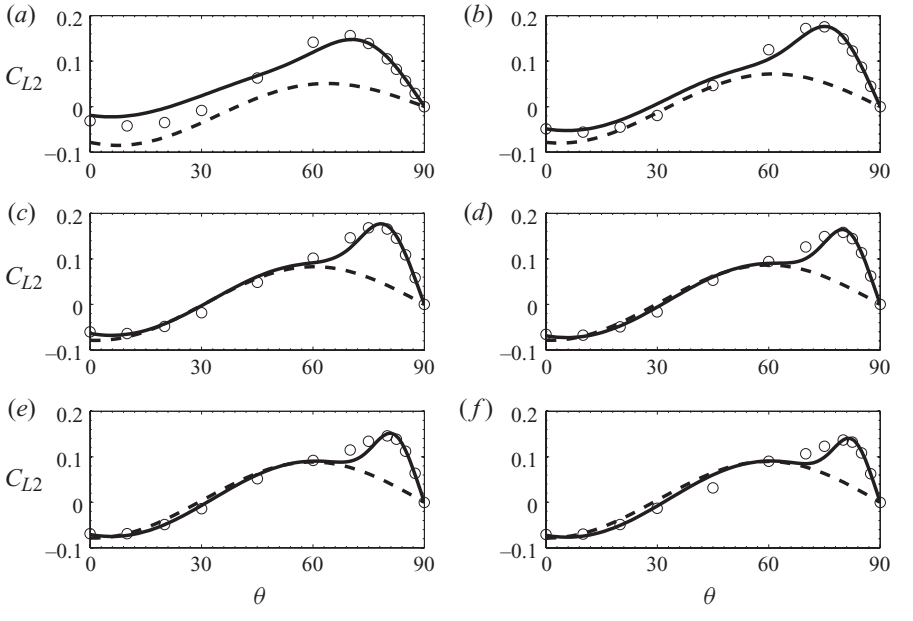


FIGURE 14. Lift coefficient C_{L2} of the trailing bubble at $S = 3$. (*a*) $Re = 20$, (*b*) $Re = 50$, (*c*) $Re = 100$, (*d*) $Re = 300$, (*e*) $Re = 400$ and (*f*) $Re = 500$. Symbols: ○, numerical results; - - -, analytical potential lift; ——, relation (6.12).

significant even if the size of the vorticity region and the size of the bubble have the same order of magnitude. This is consistent with the results of Merle *et al.* (2005), who showed that the shear-induced Auton lift force also correctly describes transverse fluctuations in a turbulent flow for bubble size comparable with the Taylor

https://doi.org/10.1017/S002211201000635X Published online by Cambridge University Press

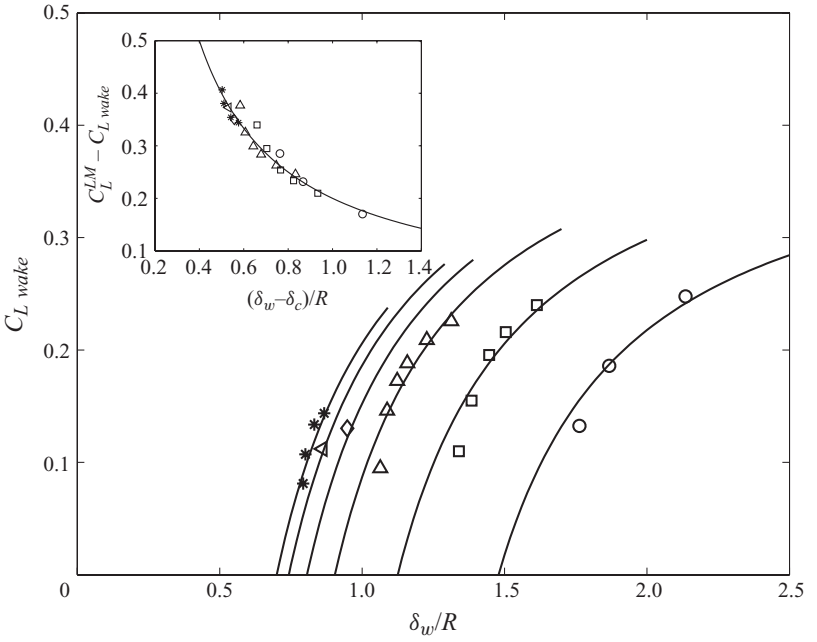


FIGURE 15. $C_{L\ wake}$ as a function of the wake width δ_w/R. Symbols: ○, $Re = 50$; □, $Re = 100$; △, $Re = 200$; ◇, $Re = 300$; ◁, $Re = 400$; ∗, $Re = 500$; ——, relation (6.14). The inset shows $C_L^{LM} - C_{L\ wake}$ as a function of $(\delta_w - \delta_c)/R$.

micro-scale of the flow. The decrease of $C_{L\ wake}$ appears to be very sharp and suggests a characteristic value δ_c corresponding to the vanishing of $C_{L\ wake}$. The inset of figure 15 reveals that it is possible to find for each Reynolds number a value for δ_c such that all the evolutions of $C_L^{LM} - C_{L\ wake}$ collapse on the same curve:

$$C_{L\ wake} = C_L^{LM} - \frac{0.2}{\delta_w - \delta_c}. \tag{6.14}$$

The characteristic size corresponding to the vanishing of $C_{L\ wake}$ is found to be well described by $\delta_c = 6.8Re^{-1/2}$. This result indicates that the induced shear lift effect vanishes when the size of the vorticity region is about the size of the vorticity boundary layer at the bubble surface.

7. Concluding remarks

This study has focused on the interaction between two spherical bubbles rising in a liquid. The interaction has been described and characterised for a large range of Reynolds numbers ($20 \leqslant Re \leqslant 500$) and separating distances ($2.5 \leqslant S \leqslant 10$) between the two bubbles. The relative position has also been described by changing the angle θ formed between the centreline and the $\boldsymbol{e}_x$-direction in order to connect previous studies performed for two bubbles rising in line (Yuan & Prosperetti 1994; Harper 1997) and for two bubbles rising side by side (Legendre *et al.* 2003). The drag and transverse (lift) forces have been analysed for each bubble and described using some simple models based on a physical description of the interaction. Note that in the present work a model of velocity field in the wake of the leading bubble was built from the results of numerical experiments and used to determine the forces exerted on the bubbles, whereas the opposite approach of assuming the external forces

https://doi.org/10.1017/S002211201000635X Published online by Cambridge University Press

on each bubble determine velocities can also be employed (e.g. Voinov & Golovin 1970; Harper 2001). The study was conducted for fixed values of θ, Re and S. The application to a real system where θ, Re and S would however vary due to the interaction forces between the two bubbles is made possible by adding to the force balance the added mass force (see Kok 1993) and by neglecting the history force that is a reasonable approximation for a spherical clean bubble moving at large Reynolds number (Magnaudet *et al.* 1995).

The interaction is the combination of three effects: the potential effect, a viscous correction (Moore's correction) and a significant wake effect observed on both the drag and the transverse forces of the second bubble when located in the wake of the first bubble. The maximum drag reduction is observed for the in-line configuration, and the maximum wake-induced lift corresponds to the maximum of $(\boldsymbol{u}-\boldsymbol{v})\times(\nabla\times\boldsymbol{u})$. Both effects have been satisfactorily described using the velocity defect, which has been characterised in the near wake of a single bubble.

The results reported indicate that the stable final position for two bubbles rising in interaction is the side-by-side configuration. The in-line configuration is thus unstable according to the negative torque whatever θ, Re and S. This agrees with the theories of Harper (1970) and Auton (1987) for the vorticity-induced lift effect on spherical bubbles with clean surfaces and with the experiments of Cartellier & Rivière (2001) at Reynolds numbers of order 10 in which there was a strong deficit in the pair density at the rear of bubbles. Nevertheless, stable lines of bubbles are often seen both in glasses of various drinks such as Champagne and in controlled experiments (Katz & Meneveau 1996; Sanada *et al.* 2005). This stability may be an effect of deformation from a spherical shape (Bunner & Tryggvason 2003; Adoua, Legendre & Magnaudet 2009) or of surface contamination (which need only be very slight; Harper 1970, 2008). Both effects are beyond the scope of this paper.

One piece of information given by the simulations reported in this paper is that, for spherical bubbly flow, the vorticity-induced lift effect experienced in wakes reinforces the potential effect that tends to form stable horizontal clusters as observed when simulating the motion of a large number of spherical bubbles in potential flow (Sangani & Didwania 1993; Smereka 1993; Yurkovetsky & Brady 1996). Such effects are not observed in three-dimensional experiments (Lance & Bataille 1991; Cartellier & Rivière 2001; Roig & Larue de Tournemine 2007; Riboux, Risso & Legendre 2010) and direct numerical simulations (Esmaeeli & Tryggvason 1998; Bunner & Tryggvason 2002). Bubbly flows are known to generate an induced agitation produced by wake interaction. Such agitation is responsible for bubble dispersion. Consequently, two mechanisms are in competition: one is the potential and wake ejection that tends to form horizontal clusters and the second is the bubble-induced agitation. Note that when the bubbly flow is forced to be two-dimensional due to wall confinement (Zenit, Koch & Sangani 2001) or because of bubble accumulation near a wall (Takagi, Ogasawara & Matsumoto 2008), some tendencies to generate clusters are observed. One possible explanation of this modification is that bubble dispersion is reduced due to the two-dimensional geometry. A criterion for bubble clustering could be proposed by comparing wake ejection and induced agitation.

Appendix. Wake of a single bubble

As described in this paper, the behaviour of the second bubble is significantly affected when located in the wake of the first bubble. The objective of this appendix

https://doi.org/10.1017/S002211201000635X Published online by Cambridge University Press

is to characterise the wake of a single bubble for the range of Reynolds number covered by this study. Here, we denote Y the radial distance from the wake axis, X the distance downstream and $r^2 = X^2 + Y^2$. A tilde denotes dimensionless quantities, R and U_∞ being used as the length and velocity scales, respectively.

At large distances downstream, the flow is known to follow the standard far-wake behaviour and the velocity deficit profile is parallel to the X-direction and is given by (Batchelor 1967):

$$u_{wake} \sim \frac{U_\infty Q}{4\pi\nu X} \exp\left[-U_\infty \frac{Y^2}{4\nu X}\right], \tag{A 1}$$

where $Q = F_{D\infty}/\rho U_\infty = C_{D\infty}\pi R^2 U_\infty/2$ is determined by integration over the wake and is directly related to the total drag $F_{D\infty}$ of the body.

In the present paper, we are considering a bubble located in the near wake of another bubble. For the distances studied ($2.5 \leqslant \tilde{X} \leqslant 10$), the far wake cannot be considered as established. At distances close to the leading bubble, the potential contribution also has a significant contribution. Following Moore's decomposition (Moore 1963), the streamwise velocity in the wake u_{wake} is expressed using the potential solution u_{pot} and a rotational perturbation u_{rot}:

$$\tilde{u}_{wake} = \tilde{u}_{X\,pot} + \tilde{u}_{rot}, \tag{A 2}$$

where $\tilde{u}_{X\,pot} = \tilde{X}^2/\tilde{r}^5 - \tilde{Y}^2/2\tilde{r}^5$ is the streamwise component of the potential flow.

Neglecting X gradients and viscous terms, Moore (1963) showed that there is a region of length $O(RRe^{1/2})$, in which the wake is of thickness $O(RRe^{-1/4})$ and where the solution for the streamwise component of the perturbation velocity is

$$\tilde{u}_{rot} = -\frac{12}{Re^{1/2}}[\pi^{-1/2}\exp(-\sigma^2) - \sigma\,\mathrm{erfc}\sigma], \tag{A 3}$$

where $\sigma = \tilde{Y}^2 Re^{1/2}/8$.

Discussing the numerical results of Yuan & Prosperetti (1994) for the in-line interaction, Harper (1997) showed that the diffusion of vorticity in the near wake cannot be neglected, and has to be considered to give a satisfactory description of the drag experienced by a second bubble, located in the wake of the first bubble. Indeed, Harper (1997) indicated that neglecting diffusion in the near wake is valid if $Re^{-1/2}\tilde{X} \ll 1$. For the Reynolds numbers ($Re = O(100)$) and the separations ($\tilde{X} = O(10)$) considered in our study, one has $Re^{-1/2}\tilde{X} = O(1)$, showing that the assumption of Moore cannot be satisfied. This is confirmed in figure 16, where Moore's solution (A 3) is compared with the numerical simulations performed for a single bubble. Several downstream distances from $\tilde{X} = 3$ to $\tilde{X} = 20$ are reported for $Re = 50$ and $Re = 500$. The simulations clearly indicate that the rotational contribution to the wake (i.e. the perturbation velocity) is dependent on X, so that Moore's assumption is not satisfied for the range of Reynolds number considered here. We also observe that the agreement with relation (A 3) is improved when increasing the Reynolds number. For $Re = 500$, we observe that $\tilde{u}_{rot}$ is reduced by 30% between $\tilde{X} = 3$ and $\tilde{X} = 6$ and divided by 3 between $\tilde{X} = 3$ and $\tilde{X} = 20$. Moore's solution overestimates the magnitude of the velocity and underestimates the width of the wake (by a factor almost 2 at $Re = 50$ and by 30% at $Re = 500$).

In order to have a simplified near-wake description that tends to the far-wake evolution given by (A 1), we propose describing the perturbation velocity of the

https://doi.org/10.1017/S002211201000635X Published online by Cambridge University Press

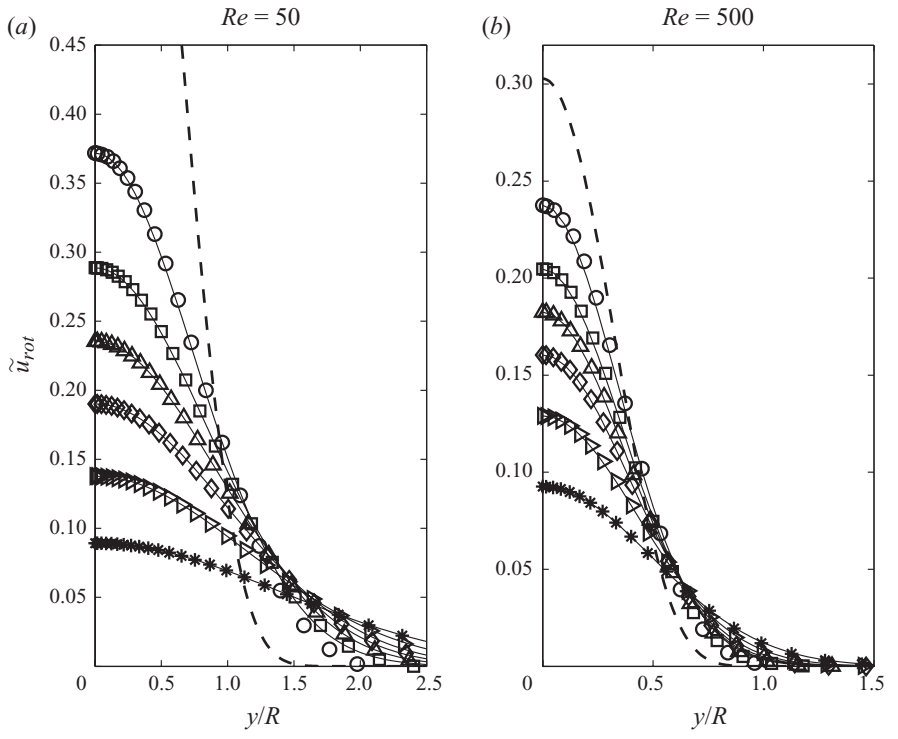


FIGURE 16. Velocity profile $\tilde{u}_{rot}$ in the near wake of a single bubble. Lines: — — —, expression (A 3); —, relation (A 4) with (α, β) given as follows. (*a*) $Re = 50$: ○, $\tilde{X} = 3$ ($\alpha = 0.533$, $\beta = 0.433$); □, $\tilde{X} = 4.5$ ($\alpha = 0.621$, $\beta = 0.515$); ◇, $\tilde{X} = 6$ ($\alpha = 0.675$, $\beta = 0.579$); △, $\tilde{X} = 8$ ($\alpha = 0.727$, $\beta = 0.644$); ◁, $\tilde{X} = 12$ ($\alpha = 0.789$, $\beta = 0.733$; ★, $\tilde{X} = 20$ ($\alpha = 0.852$, $\beta = 0.818$). (*b*) $Re = 500$: ○, $\tilde{X} = 3$ ($\alpha = 0.256$, $\beta = 0.203$); □, $\tilde{X} = 4.5$ ($\alpha = 0.331$, $\beta = 0.283$); ◇, $\tilde{X} = 6$ ($\alpha = 0.393$, $\beta = 0.399$); △, $\tilde{X} = 8$ ($\alpha = 0.461$, $\beta = 0.419$); ◁, $\tilde{X} = 12$ ($\alpha = 0.556$, $\beta = 0.527$); ★, $\tilde{X} = 20$ ($\alpha = 0.665$, $\beta = 0.650$).

wake as

$$\tilde{u}_{rot} = \frac{C_{D\infty} Re}{16} \frac{\alpha}{\tilde{X}} \exp\left[-\beta \frac{Re}{8} \frac{\tilde{Y}^2}{\tilde{X}}\right], \tag{A 4}$$

where $C_{D\infty}$ is the drag coefficient of the single bubble, which can be described using the analytical solution $C_{D\infty} = 48/Re(1 - 2.211Re^{-1/2})$ for $Re > 50$ (Moore 1963) or using the correlation $C_{D\infty} = 16/Re(16 + 3.315Re^{1/2} + 3Re)/(16 + 3.315Re^{1/2} + Re)$ for all Re (Mei, Klausner & Lawrence 1994). In expression (A 4), we have introduced two adjustable parameters α and β to fit the velocity defect of the near wake. The comparison with the numerical solution is reported in figure 16. This figure shows that at any position downstream $\tilde{X}$, it is possible to find a pair (α, β) of order unity to fit the wake profile with very good agreement. A simple fit of α and β is given by

$$\alpha = 1 - \frac{1 - 41.8Re^{-0.9} + 48Re^{-1}}{1 + \tilde{X}(1.95Re^{-0.476} - 4.5Re^{-1})}, \tag{A 5}$$

$$\beta = 1 - \frac{1.03 - 13.1Re^{-1.2}}{1 + \tilde{X}(1.33Re^{-0.409} - 3.5Re^{-1})}, \tag{A 6}$$

where (α, β) are found to tend to unity when increasing the distance, in agreement with the standard far-wake behaviour given by expression (A 1).

https://doi.org/10.1017/S002211201000635X Published online by Cambridge University Press

REFERENCES

Adoua, R., Legendre, D. & Magnaudet, J. 2009 Reversal of the lift force on an oblate bubble in a weakly viscous linear shear flow. *J. Fluid Mech.* **628**, 23–41.

Auton, T. R. 1987 The lift force on a spherical body in a rotational flow. *J. Fluid Mech.* **183**, 199–218.

Batchelor, G. K. 1967 *An Introduction to Fluid Dynamics*. Cambridge University Press.

Biesheuvel, A. & van Wijngaarden, L. 1982 The motion of pair of gas bubbles in a perfect liquid. *J. Engng Math.* **16**, 349–365.

Bunner, B. & Tryggvason, G. 2002 Dynamics of homogeneous bubbly flows. Part 1. Rise velocity and microstructure of the bubbles. *J. Fluid Mech.* **466**, 17–52.

Bunner, B. & Tryggvason, G. 2003 Effect of bubble deformation on the properties of bubbly flows. *J. Fluid Mech.* **495**, 77–118.

Cartellier, A. & Rivière, N. 2001 Bubble-induced agitation and microstructure in uniform bubbly flows at small to moderate particle Reynolds numbers. *Phys. Fluids* **13** (8), 2165–2181.

Clift, R., Grace, J. R. & Weber, M. E. 1978 *Bubbles, Drops and Particles*. Academic Press.

Endo, D. 1938 The forces on two spheres placed in a uniform flow. *Proc. Phys. Math. Soc. Japan* **20**, 667–703.

Esmaeeli, A. & Tryggvason, G. 1998 Direct numerical simulations of bubbly flows. Part 1. Low Reynolds number arrays. *J. Fluid Mech.* **377**, 313–345.

Figueroa-Espinoza, B., Legendre, D. & Zenit, R. 2008 The effect of confinement on the motion of a single clean bubble. *J. Fluid Mech.* **616**, 419–443.

Happel, J. & Brenner, H. 1965 *Low Reynolds Number Hydrodynamics*. Kluwer.

Harper, J. F. 1970 On bubbles rising in line at large Reynolds number. *J. Fluid Mech.* **41**, 751–758.

Harper, J. F. 1997 Bubbles rising in line: why is the first approximation so bad? *J. Fluid Mech.* **351**, 289–300.

Harper, J. F. 2001 Growing bubbles rising in line. *J. Appl. Math. Decis. Sci.* **5**, 65–73.

Harper, J. F. 2008 Bubbles in line: champagne, lager, cider. In *Bubbles in Food 2: Novelty, Health and Luxury* (ed. G. M. Campbell, M. G. Scanlan & D. L. Pyle), vol. 5, pp. 147–153. AACC International.

Jeffrey, D. 1973 Conduction through a random suspension of spheres. *Proc. R. Soc. Lond.* A **335**, 355–367.

Joseph, D. D. 2006*a* Potential flow of viscous fluid: historical notes. *Intl J. Multiphase Flow* **32**, 285–310.

Joseph, D. D. 2006*b* Addendum (Helmholtz decomposition) to: 'Potential flow of viscous fluid: historical notes'. *Intl J. Multiphase Flow* **32**, 886–887.

Joseph, D. D. & Wang, J. 2004 The dissipation approximation and viscous potential flow. *J. Fluid Mech.* **505**, 365–377.

Katz, J. & Meneveau, C. 1996 Wake-induced relative motion of bubbles rising in line. *Intl J. Multiphase Flow* **22** (2), 239–258.

Kim, I., Elghobashi, S. & Sirignano, W. A. 1993 Three-dimensional flow over two spheres placed side by side. *J. Fluid Mech.* **246**, 465–488.

Kok, J. B. W. 1993 Dynamics of a pair of gas bubbles moving through liquid. Part 1. Theory. *Eur. J. Mech.* B Fluids **12**, 515–540.

Lance, M. & Bataille, J. 1991 Turbulence in the liquid phase of a uniform bubbly air–water flow. *J. Fluid Mech.* **222**, 95–118.

Legendre, D. & Magnaudet, J. 1997 A note on the lift force on a spherical bubble or drop in a low-Reynolds-number shear flow. *Phys. Fluids* **9**, 3572–3574.

Legendre, D. & Magnaudet, J. 1998 The lift force on a spherical body in a viscous linear shear flow. *J. Fluid Mech.* **368**, 81–126.

Legendre, D., Magnaudet, J. & Mougin, G. 2003 Hydrodynamic interactions between two spherical bubbles rising side by side in a viscous liquid. *J. Fluid Mech.* **497**, 133–166.

Levich, V. G. 1962 *Physicochemical Hydrodynamics*. Prentice Hall.

Magnaudet, J. & Eames, I. 2000 The motion of high-Reynolds-number bubbles in inhomogeneous flows. *Annu. Rev. Fluid Mech.* **32**, 659–708.

Magnaudet, J. & Mougin, G. 2007 Wake instability of a fixed spheroidal bubble. *J. Fluid Mech.* **572**, 311–337.

https://doi.org/10.1017/S002211201000635X Published online by Cambridge University Press

Magnaudet, J., Rivero, M. & Fabre, J. 1995 Accelerated flows past a rigid sphere or a spherical bubble. Part 1. Steady straining flow. *J. Fluid Mech.* **284**, 97–135.

Mei, R., Klausner, J. & Lawrence, C. J. 1994 A note on the history force on a spherical bubble at finite Reynolds number. *Phys. Fluids* A **6**, 418–420.

Merle, A., Legendre, D. & Magnaudet, J. 2005 Forces on a high-*Re* spherical bubble in a turbulent flow. *J. Fluid Mech.* **532**, 53–62.

Moore, D. W. 1963 The boundary layer on a spherical gas bubble. *J. Fluid Mech.* **16**, 161–176.

Riboux, G., Risso, F. & Legendre, D. 2010 Experimental characterization of the agitation generated by bubbles rising at high Reynolds number. *J. Fluid Mech.* **643**, 509–539.

Roig, V. & Larue de Tournemine, A. 2007 Measurement of interstitial velocity of homogeneous bubbly flows at low to moderate void fraction. *J. Fluid Mech.* **572**, 87–110.

Sanada, T., Watanabe, M., Fukano, T. & Kariyasaki, A. 2005 Behavior of a single coherent gas bubble chain and surrounding liquid jet flow structure. *Chem. Engng Sci.* **60**, 4886–4900.

Sangani, A. S. & Didwania, A. K. 1993 Dynamic simulations of flows of bubbly liquids at large Reynolds number. *J. Fluid Mech.* **250**, 307–337.

Smereka, P. 1993 On the motion of bubbles in a periodic box. *J. Fluid Mech.* **254**, 79–112.

Takagi, S., Ogasawara, T. & Matsumoto, Y. 2008 The effects of surfactant on the multiscale structure of bubbly flows. *Trans. R. Soc.* A **366**, 2117–2129.

Voinov, O. V. & Golovin, A. M. 1970 Lagrange equations for a system of bubbles of varying radii in a liquid of small viscosity. *Fluid Dyn.* **5**, 458–464.

van Wijngaarden, L. 1976 Hydrodynamic interaction between gas bubbles in liquid. *J. Fluid Mech.* **77**, 27–44.

Yuan, H. & Prosperetti, A. 1994 On the in-line motion of two spherical bubbles in a viscous fluid. *J. Fluid Mech.* **278**, 325–349.

Yurkovetsky, Y. & Brady, J. F. 1996 Statistical mechanics of bubbly liquids. *Phys. Fluids* **8** (4), 881–895.

Zenit, R., Koch, D. L. & Sangani, A. S. 2001 Measurements of the average properties of a suspension of bubbles rising in a vertical channel. *J. Fluid Mech.* **429**, 307–342.

https://doi.org/10.1017/S002211201000635X Published online by Cambridge University Press